Microelectronics Reliability 114 (2020) 113888

Contents lists available at ScienceDirect

Microelectronics Reliability

journal homepage: www.elsevier.com/locate/microrel

A lifetime assessment and prediction method for large area solder joints

M. Lederer, A. Betzwar Kotas, G. Khatibi*

Christian Doppler Laboratory for Lifetime and Reliability of Interfaces in Complex Multi-Material Electronics, Institute of Chemical Technologies and Analytics, Vienna Universtity of Technology, Getreidemarkt 9/164 1060 Vienna, Austria

A B S T R A C T

Mechanical bending fatigue experiments were conducted on large area Pb-rich and SnSb-based model solder joints consisting of Cu-strip/solder/DCB substrates. Experimental lifetime curves in the range between 10^5 and 10^8 loading cycles at room and elevated temperature showed an improved fatigue resistance for SnSb alloys. Crack length as a function of loading cycles (da/dN) was determined for selected samples to study the cyclic degradation behaviour of the solder layer. Crack initiation and propagation in the joints was modelled on the basis of a damage accumulation rule considering the strain rate and temperature dependency of the solder alloy. Application of the FEM model to large area solder joints allowed calculation of the incremental advancement of the crack front, determination of the crack growth rate (da/dN) and prediction of lifetime under a given loading condition.

1. Introduction

In advanced high power semiconductor modules with robust wire bonding technologies solder joints are still considered as the most vulnerable site of the devices. In this context, extensive research is ongoing to develop alternative interconnection materials for high temperature applications [1,2]. The reliability of solder interconnects is mainly affected by thermomechanical fatigue which occurs due to combination of temperature cycling and thermal mismatch between the two joining parts for example in the solder die attach connecting the chip to the substrate or the large area solder layer between the substrate and the baseplate. The high homologous temperatures during the operation induce considerable stresses in the solder joints which, together with the contribution of creep fatigue and microstructural modifications caused by diffusion processes, lead to initiation and propagation cracks and fatigue failure of the solder joints [3,4].

In industrial practice accelerated power or thermal cycling tests are conducted to assess the thermomechanical reliability of devices and to establish lifetime curves. While die attach solders are more affected during the PC tests, thermal cycling tests, which provide a homogeneous distribution of temperature in the devices are commonly used for evaluation of substrate solder joints. Considering the inhomogeneous structure and the viscoplastic behaviour of the solders under typical operational temperatures, determination of failure mechanisms and prediction of lifetimes are complicated. A number of studies have shown that variation of testing conditions may strongly affect the lifetime and dominant failure modes in the devices [5,6]. Thus, establishment of reliable lifetime prediction models requires a deep knowledge and understanding of the time and temperature dependent deformation behaviour of the solders and the stress-strains conditions in the joints. Consequently, the static and cyclic properties of the solder joints have been subject of a large number of studies. Isothermal fatigue tests at low and moderate testing frequencies have been conducted for extraction of data for constitutive models, validation of finite element simulations and establishment of lifetime prediction models.

In a different approach, isothermal mechanical fatigue testing has been proposed as an alternative to thermal cycling for accelerated lifetime assessment of solder joints. In previous studies, the authors proposed a high frequency isothermal bending fatigue testing method for rapid evaluation of solder joints by using model multi-layered structures [7]. By applying this testing procedure lifetimes of Pb-rich chip/solder/substrate test structures were obtained while failure modes similar to those observed in service could be reproduced.

In the present study the proposed method has been applied to study the degradation rate and lifetime of two types of Pb-rich and Pb-free solder joints used in power semiconductor modules. Finite element modelling (FEM) is applied to calculate the distribution of stress and strain in the test structures and modelling of the crack initiation and propagation leading to failure of the joints by using the boundary conditions of the mechanical fatigue tests and the experimental fatigue data.

2. Experimental

2.1. Sample preparation

Two types of Pb rich and Pb-free solder alloys which are commonly

* Corresponding author.
E-mail address: golta.khatibi@tuwien.ac.at (G. Khatibi).

https://doi.org/10.1016/j.microrel.2020.113888
Received 1 June 2020; Received in revised form 10 July 2020; Accepted 24 July 2020
Available online 31 October 2020

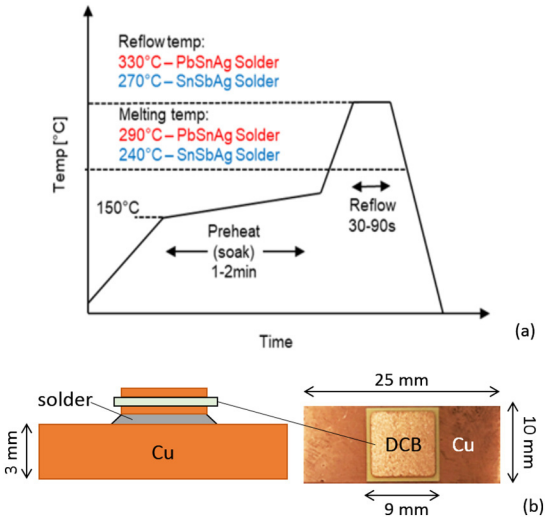

Fig. 1. Schematic reflow profile for PbSnAg and SnSbAg Solder (a) cross section and top view of DCB/solder/Cu model joints (b).

used in high power electronic devices were used for preparation of solder joints. Model test structures were fabricated by using thin foils of PbSnAg and SnSbAg solder with a thickness of about 100 µm to join copper strips (3 × 10 × 25 mm) and commercial direct bonded copper (DCB) square plates (9 × 9 mm). The thicknesses of the Cu metallization layers and the Al_2O_3 ceramic were 300 µm and 320 µm respectively. It is known that the adhesion properties, failure mode and crack growth behaviour of the bonded joints are affected by the surface conditions of the joining parts [8,9]. In this study the surface of copper strips was ground by 1200, 2400 and 4000 grade silicon carbide papers and subsequently washed with deionized water and anhydrous alcohol. Plates of DCB were used as fabricated and washed with Ethanol before the soldering process. The sample preparation method was selected to achieve an optimized wetting of the Cu surfaces during the reflow. The samples were reflowed at a temperature of about 330 °C for Pb-rich and 270 °C for the Pb-free solder resulting in joints with gap sizes in the range of 40-50 µm (Fig. 1). Solder joints for shear testing were prepared by using the same procedure. In this case to avoid fracture of the ceramic during the shear testing, the substrates were replaced by Cu pieces with dimensions of 5 × 5 × 2 mm. The results of shear tests which were conducted at room temperature and 80 °C are given in Table 1 showing considerably higher values of the lead-free alloy.

Metallographic sections were prepared to reveal the microstructure of the solder joints as shown in Fig. 2. The PbSnAg joints consisted of a Pb-reach solid solution with βSn grains and fine Ag_3Sn particles with a thin Cu_3Sn intermetallic layer at the interface of solder to copper (Fig. 2a). The microstructure of the SnSbAg solder which contained a high weight percentage of Sn, consisted of a Sn solid solution matrix with SnSb grains and fine precipitates of Ag_3Sn (Fig. 2b).

2.2. Fatigue testing method

Isothermal three-point bending fatigue tests were performed by using an ultrasonic resonance fatigue testing equipment operating at a frequency of 20 kHz. The testing system consists of a power supply, a piezoelectric transducer and an acoustic horn with a tip. The 3-point bending configuration consists of the multi-layered resonant sample which is placed on two steel supports below the tip of the acoustic horn. The fatigue test is started after applying a small pre-load to the back side of the substrate with the tip of the acoustic horn. The resonance sample is excited to sinusoidal transversal vibrations at a constant a displacement amplitude as shown schematically in Fig. 3. The displacement amplitude of the sample during the loading was measured by using a laser Doppler vibrometer (LDV). The failure criteria for this series of samples was full detachment of the DCB from the substrate with the runout limit being $N = 1e8$ loading cycles. The time to failure was determined by monitoring the entire experiments with a digital microscope. Fatigue tests at elevated temperatures were performed by using a heating chamber. The dimensions of the resonance multi-layered samples were determined by means of FEM. Details of the fatigue testing system is described in [7].

The load levels chosen in the bending fatigue tests were somewhat higher than thermomechanical loads expected under service conditions. Insofar, the results of lifetime tests reflect the material response to overstress. However, the change of microstructure as a result of long term thermal exposure was not covered by this accelerated test method.

Table 1
Shear stress of the solder joints.

Samples	Shear stress at RT [MPa]	Shear stress at 80°C [MPa]
Cu/PbSnAg/Cu	38	21
Cu/SnSbAg/Cu	52	38

3. Results

3.1. Lifetime curves

The end of life curves of the two types of model solder joints obtained at displacement amplitudes of 4 to 6 µm in the range from 1e5 to 2e8 loading cycles are presented in Fig. 4a, b.

The data were obtained at ~23 °C (RT) and 80 °C for the Pb-rich solder joints (Fig. 4a) and at 80 °C for the lead free solder (Fig. 4b). It should be mentioned that cyclic loading of SnSbAg solder joints at room temperature resulted in a change of failure mode from solder fatigue to delamination of Cu-metallization from the Al_2O_3 layer at stress levels below 6 µm. Accordingly, these data are not included to the plots. Fatigue loading at 80 °C resulted in delamination in the joints and failure due to separation of the DCB from the substrate. The fatigue data of the Pb-rich samples at two testing temperatures reveal a considerable decrease in fatigue resistance at 80 °C. The plots in Fig. 4b provide a comparison between the fatigue performance of the Pb-rich solder joints with that of PbSnAg joints at 80 °C. The data show a considerably higher fatigue resistance of these joints under the given testing conditions as discussed later in this paper. The beneficial effect of Sb addition to Sn-based solders has been also reported in other studies [10,11].

In a second approach, the stages of crack initiation and propagation in the solder layer during the cyclic bending loading was studied in order to gain a better understanding on the degradation behaviour of the solder joints before end of life. These studies were conducted by examination of the side surface of the solder joints during the intermittent loading and measurement of the crack length after certain number of loading cycles. The experimental data were used for modelling of the crack growth behaviour of the large area joints as described in the next section. Furthermore, the fatigue fracture surfaces of the joints after fatigue failure were evaluated.

The location of fatigue crack initiation and crack growth path in the solder layer in a Cu/PbSnAg/DCB joint is presented in the cross-sectional image in Fig. 5a. The cracks always initiated at the four corners of the joints, and then grew from both sides of the DCB into the solder layer (Fig. 5b). With increasing the loading cycle and gradual decrease of the contact area to about 30% failure occurred in most cases abruptly due to separation of the DCB from the substrate. However, at low displacements amplitudes and number of loading cycles up to 1e8 which was set as run-out limit, final separation of the DCB from the substrate was not always observed. Subsequent cross sectioning of the samples revealed as well degradation of the solder layer and cracking in these samples. The retardation in fatigue failure of degraded joints can be related to a very slow crack growth rate in the solder layer at low

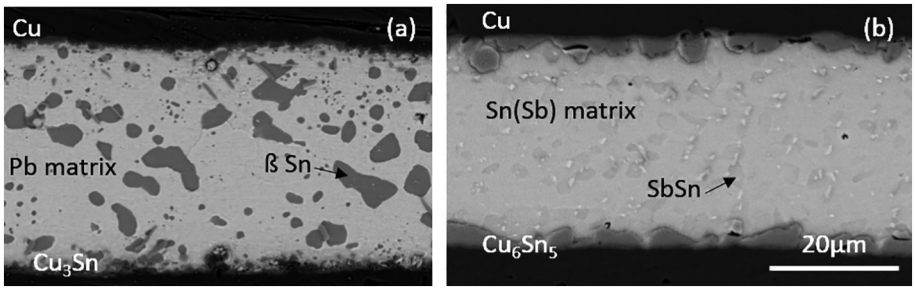

Fig. 2. Microstructure of PbSnAg (a) and SnSbAg (b) solder joints.

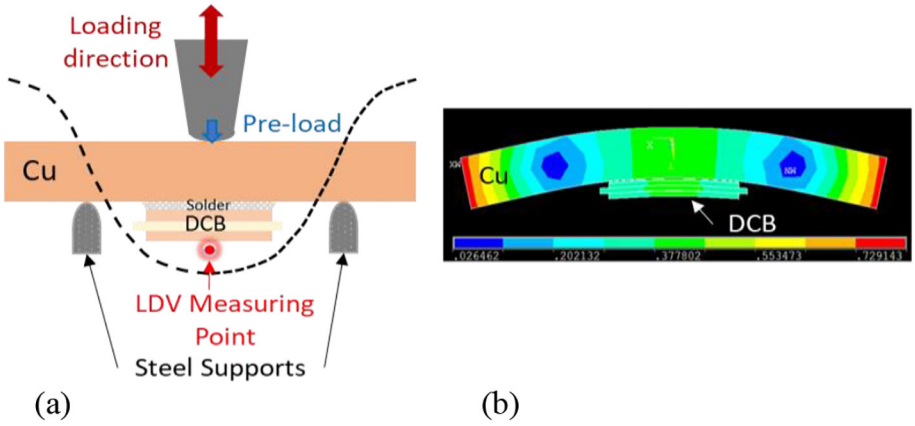

Fig. 3. Schematic of fatigue loading (a), Displacement plot of a sample subjected to bending fatigue (b).

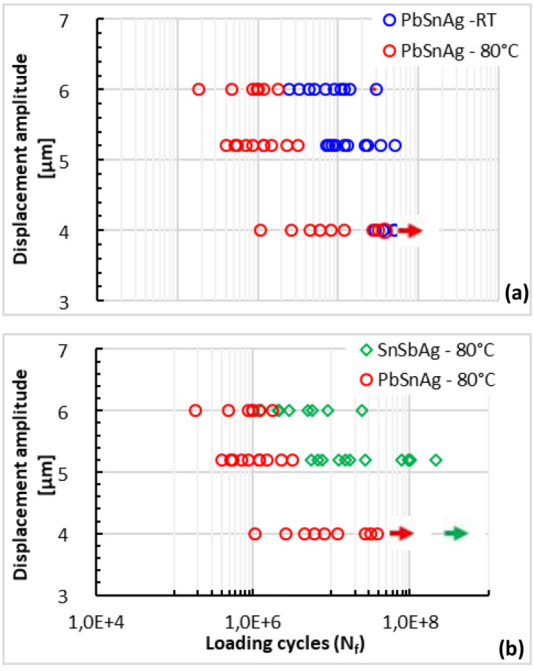

Fig. 4. Cyclic bending fatigue life curves of PbSnAg and SnSbAg solder joints at room temperature and 80 °C.

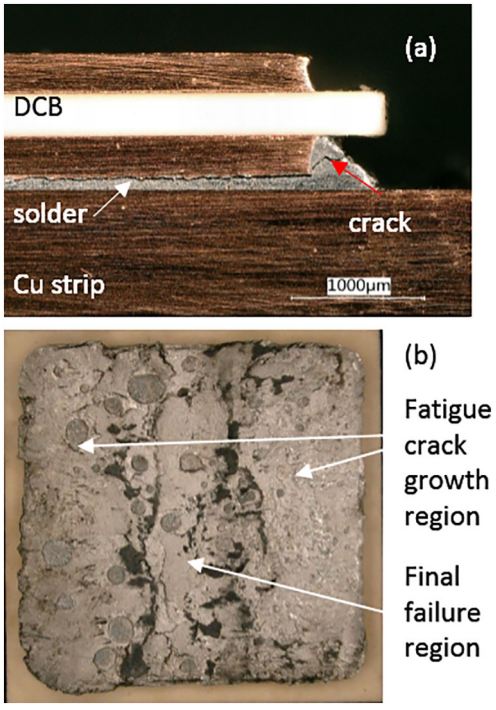

Fig. 5. Cross section of a DCB/solder/Cu multilayer showing a fatigue crack within the solder joint a) fracture surface at the DCB side revealing the fatigue crack propagation region at both sides and the final fracture area in the middle of an SbSnAg joint.

displacement amplitudes.

3.2. Finite element modelling

The lifetime data collected from cyclic bending tests are now utilized to establish a lifetime model, which is applicable to arbitrary loading scenarios. Fig. 4 shows the number of loading cycles to failure in dependence of the displacement amplitudes. However, a representation of fatigue life in dependence of applied stresses or stress intensities is here desired. Therefore, transient FEM simulations of the cyclic bending experiments were performed with ANSYS 19 using

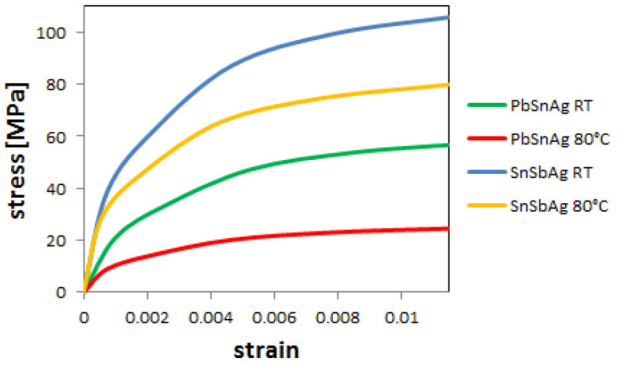

Fig. 6. Material models for solders at room temperature and 80 °C at a strain rate of $4 \cdot 10^2 \mathrm{sec}^{-1}$.

Table 2
Young's moduli for the solder materials at room temperature and at 80 °C.

	E [GPa] at RT	E [GPa] at 80 °C
PbSnAg	21	20.2
SnSbAg	52	50

multilinear kinematic hardening material models for the solders. The stress-strain curves for the solder materials at room temperature and 80 °C for strain rates of $4 \cdot 10^2 \mathrm{sec}^{-1}$, as depicted in Fig. 6, were obtained from extrapolation of strain rate dependent literature data. The temperature dependent Young's moduli of the solder materials assumed in the simulation are given in Table 2. Material data for the solder alloys may be found in references [12, 13].

Lifetime models for large area solder joints usually consist of predictions for the time to crack initiation together with an assessment of the crack propagation rate. In the range of up to 10^5 loading cycles to failure, the Darveaux model [14] has often been preferred. This model relates the time to crack initiation and the crack propagation rate to the plastic energy density. In the present study, however, fatigue data were collected in the high cycle regime of up to 10^8 loading cycles to failure. In this range, crack initiation can occur without preceding plastic deformation. Hence, the time to crack initiation N_0 is here modelled according to the equation

$$N_0 = c_1 \bullet {\varepsilon_{tot}}^b \tag{1}$$

where c_1 and b are material constants, and ε_{tot} is the total mechanical von Mises strain. This approach is based on a similarity to the Engelmaier model [3], which relates the number of loading cycles to failure to the total mechanical shear strain.

On the other hand, the evaluation of the crack propagation rate is here complicated due to the strain rate dependence of the solder material. Consideration of the strain rate dependence in the elasto-plastic material model implies high stresses. Consequently, high plastic energy densities are observed in the solder materials during simulation of cyclic bending experiments at 20 kHz. If one applies an approach in the style of the Darveaux model together with material parameters determined through experiments at low strain rates, then the theoretical crack propagation rates for simulations at high strain rates appear overestimated compared to experimental values. In order to derive some improvement, it is here suggested to model the crack propagation rate as

$$\frac{da}{dN} = c_2 \bullet {\Delta\varepsilon_{pl}}^d \tag{2}$$

where the power law for the crack propagation rate da/dN [mm] is related to the plastic strain instead of using a relationship to the plastic energy density. Thereby, c_2 and d are temperature dependent material parameters. An approach of this kind can be justified on the basis of damage mechanics: In the theory of damage mechanics, it is common place to assume a critical value of accumulated plastic strain to failure [15–17]. Usually, the implementation of damage mechanics in FEM simulations involves deletion of elements, when a critical value of accumulated strain is reached. Thereby, the whole time scale of an experiment is simulated. This is not possible here, owing to the very large number of loading cycles. Therefore, the calculation of crack propagation rates is here preferred to a methodology of consecutive element deletion. In conclusion, the path of crack propagation is calculated in incremental steps, where the contours of the plastic strain distribution of a previous step are used to predict the frontline of the ongoing crack in the subsequent step. The evaluation of crack paths by extrapolation of crack propagation rates is here considered as approximation, whereby the computational costs were reduced in the sense that only a few loading cycles were simulated explicitly:

After every extension of the crack front consistent with da/dN values of the previous increment, the FEM model of the new sample is reconstructed according to a parametrized model of the crack line geometry. This leads to the consequence that the accumulated plastic strain and the initial velocities of material points are set back to zero at the beginning of every new increment of crack propagation. Therefore, the first three periods of oscillation of the transient simulation cannot be considered as representative for the steady state solution of the dynamic model. Instead, it is always the fourth period of oscillation, which is used for evaluation of the plastic strain increment $\Delta\varepsilon_{pl}$. Thereby, the periodical accelerations applied to the contact area between ultrasonic horn and sample were adjusted in order to reach the experimentally measured displacement amplitudes during this fourth period of oscillation. In this context, the static preload supplied to the sample was included in the simulation in accordance with the experimental setup.

At this point, it should also be mentioned that the plastic strain ahead of the crack tip is mesh size dependent. The stress concentration at the crack tip was averaged over the volume of an element. Insofar, the present model uses the same method of volume averaging as the Darveaux model. Therefrom, one obtains a computational inexpensive method of evaluating fracture mechanical aspects of crack growth. The results obtained from simulation of mechanical experiments at high strain rates may be transferred to thermal cycling at low strain rate, when equivalent mesh sizes are used. In order to estimate the numerical errors arising from mesh size dependence, a mesh convergence study was performed. For this purpose, the element size dependence of the accumulated plastic strain per loading cycle was evaluated for samples exposed to 6 µm displacement amplitude at 80 °C for crack lengths of 200 µm, respectively. Results are depicted in Fig. 7. It may me

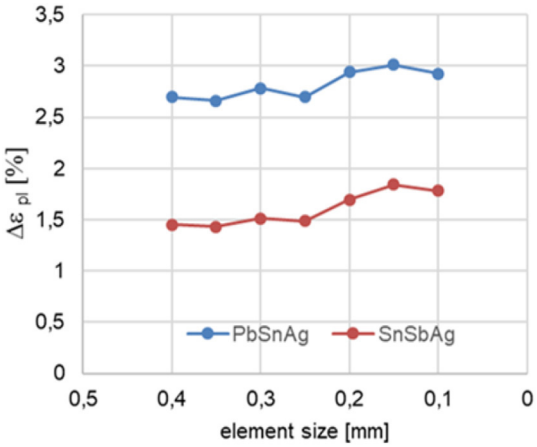

Fig. 7. Plot of accumulated plastic strain per loading cycle at the crack tip versus element size. The samples had crack lengths of 200 µm and were exposed to displacement amplitudes of 6 µm at 80 °C, respectively.

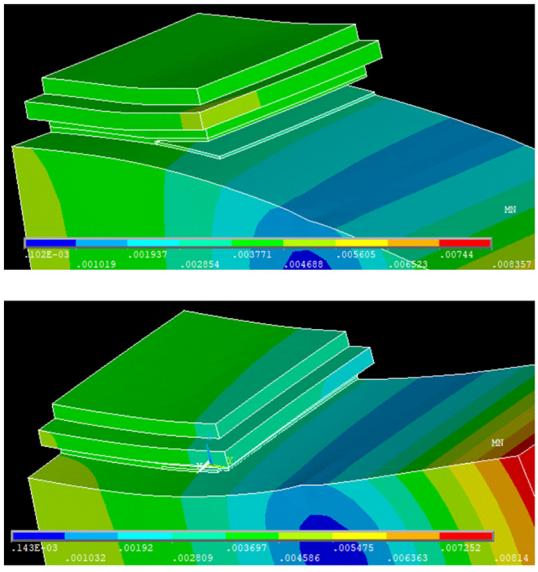

Fig. 8. Plot of the displacement vector sum [mm]. Time step, where crack opening takes its maximum (a). Time step of crack closure (b). A sample with 1.4 mm crack length in the SnSbAg solder joint is shown.

Table 3
Material parameters used for modelling of crack initiation and crack propagation [mm/cycles].

	c_1	b	c_2	d
PbSnAg-RT	2.5	−2.5	42	4.1
PbSnAg-80 °C	$3.9 \cdot 10^{-3}$	−3.82	6.5	3.9
SnSbAg-RT	0.29	−3.1	$1.5 \cdot 10^{6}$	7.1
SnSbAg-80 °C	$7.7 \cdot 10^{-5}$	−4.5	$2.1 \cdot 10^{4}$	6.1

concluded that variation of the element size by a factor of 4 does not alter the model predictions significantly. The present FEM simulations of bending fatigue involved the use of ANSYS contact elements TARGE 170 and CONTA 174. The contact elements shared the material properties of the solder. Furthermore, a friction coefficient of 0.1 was assumed for gliding of contacting areas. However, the main portion of contact interaction was due to normal forces avoiding penetration of crack flanks. The mesh of the solder material was constructed with SOLID 186 tetrahedral elements of 100 µm element size. During vibration, the crack flanks opened and closed periodically.

Thereby, unphysical overlapping of volumes during crack closure was avoided. The deformation mode shape of crack opening and crack closing is depicted in Fig. 8. In fact, the contact phenomena had a significant influence on the evolution of stresses and strains at the crack tip.

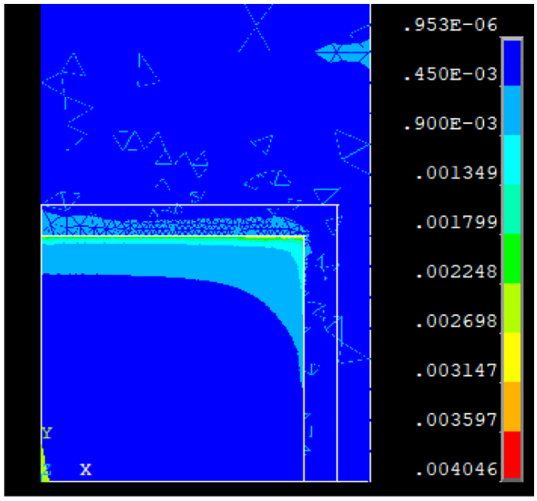

Fig. 10. Cut view through the solder layer. Plot of the total von Mises strain for the time step, where it takes its maximum. The sample is the same as in Fig. 9.

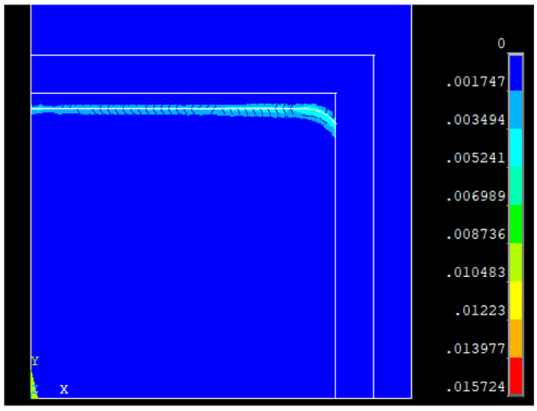

Fig. 11. Plot of the accumulated plastic strain for the last time step of the current crack propagation increment. The sample is the same as in Figs. 9 and 10, but a crack front has already been initiated.

The material parameters c_2 and d, which are needed for evaluation of crack propagation rates, can be determined by analogy to the method used for the Darveaux model [14]. The overall lifetime N_f of the sample may be written in the form

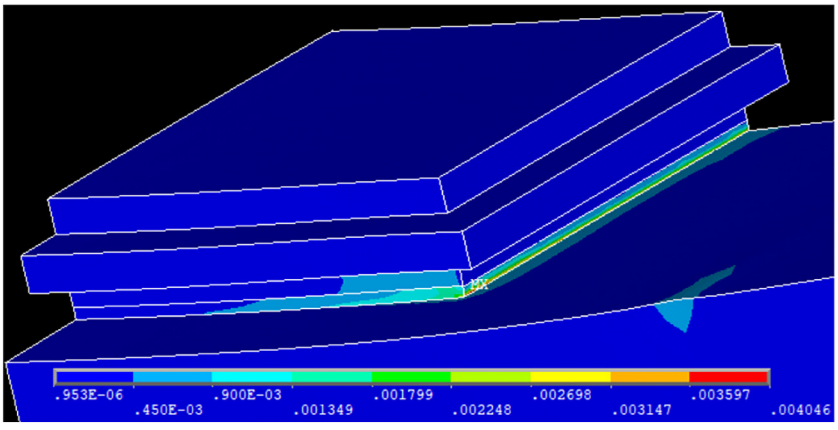

Fig. 9. Plot of the total von Mises strain for the time step where it takes a maximum. Sample soldered with SbSnAg at 5 µm displacement amplitude is shown.

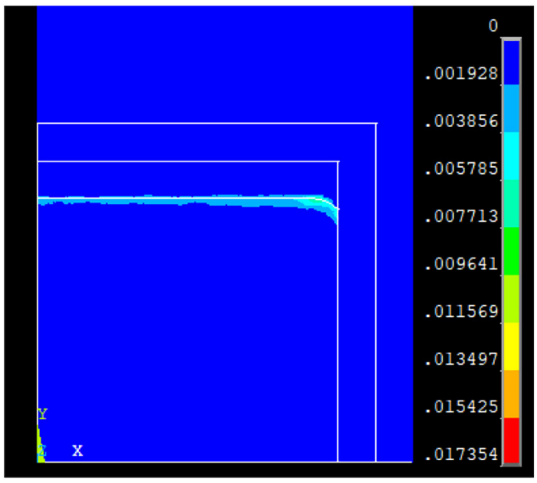

Fig. 12. Plot of accumulated plastic strain. The crack has further advanced compared to the previous Fig. 11.

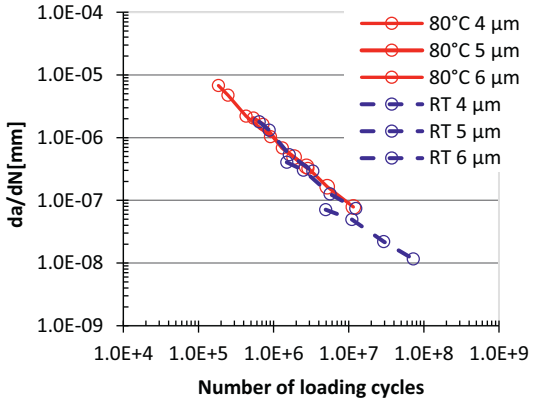

Fig. 13. Crack propagation rates for the PbSnAg solder at room temperature in dependence of vibration amplitude and number of loading cycles.

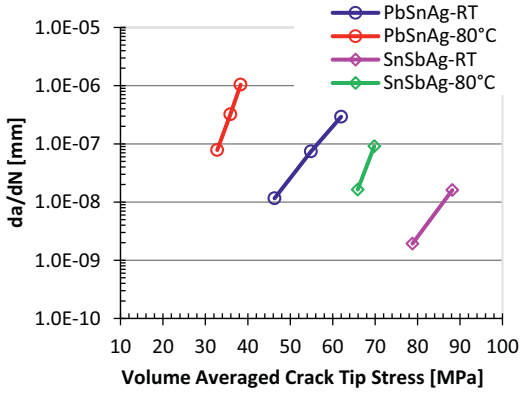

Fig. 14. Crack propagation rate plotted versus crack tip stress, whereby the stresses were averaged with respect to the element size.

$$N_f = N_0 + \int_0^{a\,final} \frac{dN}{da} da \tag{3}$$

where dN/da is the inverse of the crack propagation rate given in Eq. (2). Further, the integral of Eq. (3) may be approximated by the sum

$$N_f = N_0 + \sum \frac{\Delta N}{\Delta a}\Delta a = N_0 + \sum \frac{\Delta a}{c_2 \cdot \Delta\varepsilon_{pl}{}^{d}} \tag{4}$$

whereby the infinitesimal crack extensions da are replaced by

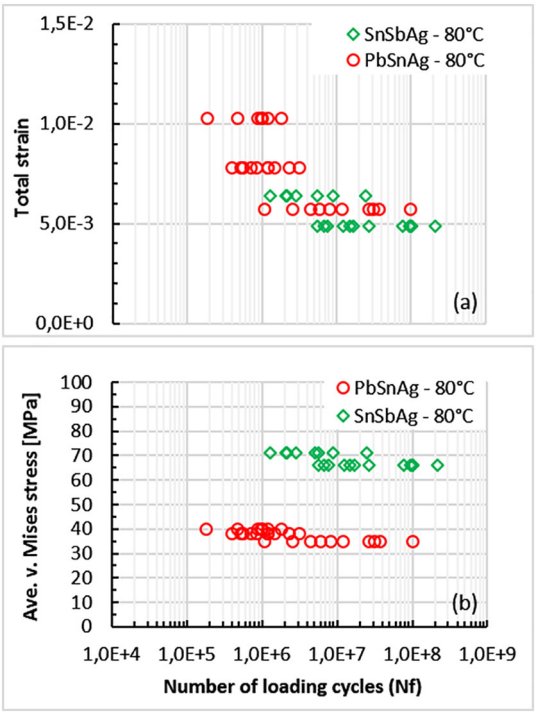

Fig. 15. Relation between the overall lifetime N_f of the sample with total mechanical strain (a) and the volume averaged stress (b) leading to crack initiation at N_0, respectively.

increments Δa of finite length. Thus, the increments of plastic strain per loading cycle, $\Delta\varepsilon_{pl}$, determined by FEM simulation at the tips of cracks with lengths a are inserted into Eq. (4). The simulated lifetime of the sample ends, when the crack path reaches a length equivalent to half of the solder joints length, because due to a symmetry condition, a second crack is expected to propagate along the opposite direction. The optimized model parameters for PbSnAg and SnSbAg solder joints are summarized in Table 3.

For clarity, the simulation procedure for calculation of the crack path is here explained in more detail: In the initial state, a defect free sample was assumed. Due to symmetry conditions, only a quarter of a sample was simulated. In view of the criterion represented by Eq. (1) the time N_0 to crack initiation was deduced from a plot of the total von Mises strain, as shown in Fig. 9 for one selected sample.

Thereby, that time step of the transient analysis was considered, where the total mechanical strain in the solder took its maximum. Crack initiation started at the corner of the solder joints, where the highest strain values were found. In consequence, the parameters c_1 and b of Eq. (1) could be determined by comparison of ε_{tot} with experimental data observed for N_0. The frontline of the crack assumed for the subsequent increment was obtained from a cut view of the previous increment by considering the precise shape of the plot for total mechanical strains, as depicted in Fig. 10. It should be recognized that the contours of the total mechanical strain in the solder show a smooth and rounded shape at the corners. Thereupon, the second increment representing the propagation of the crack line was simulated, whereby the newly generated crack flanks were covered with contact elements.

Thereafter, the frontline of the propagating crack was determined from cut views of contour plots for the accumulated plastic strain. Strictly speaking, the increment of accumulated plastic strain per loading cycle was considered. By repetition of this procedure, the crack path was derived from a sequence of incremental steps predicting crack propagation rates, as depicted for the example of two consecutive steps in Figs. 11 and 12. In conclusion, the temperature dependent material parameters c_2 and d could be determined according to Eq. (4) by

comparing the simulation results for $\Delta\varepsilon_{pl}$ on the one hand with the experimental observations for lifetimes and crack propagation on the other.

The evolution of the crack propagation rate da/dN depends on the load level, on the crack length a and on the elastic modulus of the solder material. Graphical representations of crack propagation rates da/dN versus number of loading cycles are depicted in Fig. 13 for the case of PbSnAg solder joints. The crack propagation rate may also be plotted in dependence of the volume averaged crack tip stress, as shown in Fig. 14 for the case of a 1400 μm long crack.

The plots show that a given crack growth rate considerably higher stresses at the crack front are required to induce delamination in the SnSbAg joint compared to the Pb rich solder. To provide a comparison between the lifetime curves of the Pb-rich and SnSbAg solder in terms of the calculated strain and stress values, the experimental lifetime curves in Fig. 4 have been displayed either as a function of total strain (Fig. 15a) or as function of averaged v. Mises stress (Fig. 15b). It should be noted that according to Eq. (1) the given stress and strain values are valid for the initiation of the cracks at N_0 and vary with increasing the crack length. The plots reveal a remarkably higher fatigue resistance for the SnSbAg solder material at high cycle regime which is attributed to the high stiffness and creep resistance of the Sb containing solder alloy [10,11,13].

4. Summary and conclusions

High frequency isothermal fatigue tests were applied to determine the lifetime of large area solder joints during cyclic bending loading. Depending on the vibration amplitude, overall lifetimes in the range between 10^5 and 10^8 loading cycles were observed. In order to relate the displacement amplitudes of the experiment to stresses and strains in the solder material, FEM simulations were performed. The time to crack initiation and the crack propagation rate were successfully simulated according to a modified Darveaux model. A dependence of the crack propagation rate on the crack length was found showing a reduction of the crack propagation rate during the fatigue test. A comparison between PbSnAg and SnSbAg solders showed that both materials fail at similar values of total mechanical strain, but due to the higher Young's modulus, the SnSbAg solder can withstand much higher stresses. However, the estimation of the overall lifetime is complicated by the time evolution of stresses and crack propagation rates. Therefore, the time to crack initiation N_0 and the crack propagation rate da/dN must both be considered in detail, when the lifetime model shall be applied to arbitrary loading scenarios. In the case that fatigue data obtained from ultrasonic tests are applied to thermal cycling, the consideration of the strain rate dependence of the solder is essential. Thereby, the lifetime parameters of Table 3 may be used in combination with elasto-plastic stress strain curves for solder materials at the associated strain rates, respectively.

CRediT authorship contribution statement

M. Lederer: Conceptualization, Methodology, Visualization, Writing - original draft, Writing - review & editing. **A. Betzwar Kotas**: Methodology, Visualization, Writing - review & editing. **G. Khatibi**: Conceptualization, Visualization, Writing - original draft, Writing - review & editing, Funding acquisition, Project administration.

Declaration of competing interest

The authors declare that they have no known competing financial interests or personal relationships that could have appeared to influence the work reported in this paper.

Acknowledgements

The financial support by the Austrian Federal Ministry for Digital and Economic Affairs and the National Foundation for Research, Technology and Development is gratefully acknowledged.

References

[1] K. Siow, Die-Attach Materials for High Temperature Applications in Microelectronics Packaging, Springer, 2019.
[2] N. Heuck, R. Bayerer, S. Krasel, F. Otto, R. Speckels, K. Guth, (2015). 321–324. https://doi.org/10.1109/ISPSD.2015.7123454.
[3] W. Engelmaier, IEEE Trans. Compon. Packag. Manuf. Technol. 6 (1983) 232–237.
[4] P. Lall, et al., IEEE Trans. Ind. Electron. 58 (/7) (2011) 2605–2616.
[5] T. Hunger, R. Bayerer, PCIM, (2009), pp. 713–716.
[6] M. Junghaenel, U. Scheuermann, Microelectron. Reliab. 76–77 (2017) 480–484.
[7] G. Khatibi, A. Betzwar Kotas, M. Lederer, Microelectron. Reliab. 85 (2018) 1–11.
[8] S. Kashi, M. Keshavarz, D. Vasilevskiy, R. Masut, S. Turenne, J. Electron. Mater. 41 (2012).
[9] P.C. Mohaparata, L.V. Smith, SAMPE Conference Proceedings, (2017), pp. 1–14.
[10] P. Dietrich, Microelectron. Reliab. 54 (2014) 1901–1905.
[11] A. Morozumi, H. Hiroaki, Y. Nishimura, E. Mochizuki, Y. Takahashi, Trans. Jpn. Inst. Electron. Packag. 8 (2015) 8–17, https://doi.org/10.5104/jiepeng.8.8.
[12] S.A. Gupta, Temperature and Rate Dependent Partitioned Relationships for 95.5Pb2Sn2.Ag Solder Alloy, PhD thesis University of Maryland, 2003, pp. 64–66 pages.
[13] A.R. Geranmayeh, R. Mahmudi, M. Kangooie, Mater. Sci. Eng. A 528 (2011) 3967–3972.
[14] R. Darveaux, Solder joint fatigue life model, Proc. TMS Annual Meeting, Orlando, FL, 1997, pp. 213–218.
[15] J. Lemaitre, A Course on Damage Mechanics, Springer, Berlin, New York, 1992.
[16] L. Xue, Int. J. Solids Struct. 44 (2007) 5163–5181.
[17] Z.S. Hosseini, M. Dadfarnia, B.P. Somerday, P. Sofronis, R.O. Ritchie, J. Mech. Phys. Solids 121 (2018) 341–362.